



HAL
open science

Enhanced magnetocrystalline anisotropy in an ultra-dense array of air-exposed crystalline cobalt nanowires

I. S Camara, Charbel Achkar, Nikolaos Liakakos, Alexandre Pierrot, V. Pierron-Bohnes, Y. Henry, K. Soulantika, Marc Respaud, Thomas Blon, M. Bailleul

► To cite this version:

I. S Camara, Charbel Achkar, Nikolaos Liakakos, Alexandre Pierrot, V. Pierron-Bohnes, et al.. Enhanced magnetocrystalline anisotropy in an ultra-dense array of air-exposed crystalline cobalt nanowires. *Applied Physics Letters*, 2016, 109 (20), pp.202406. hal-01989562

HAL Id: hal-01989562

<https://hal.insa-toulouse.fr/hal-01989562>

Submitted on 22 Jan 2019

HAL is a multi-disciplinary open access archive for the deposit and dissemination of scientific research documents, whether they are published or not. The documents may come from teaching and research institutions in France or abroad, or from public or private research centers.

L'archive ouverte pluridisciplinaire **HAL**, est destinée au dépôt et à la diffusion de documents scientifiques de niveau recherche, publiés ou non, émanant des établissements d'enseignement et de recherche français ou étrangers, des laboratoires publics ou privés.

Enhanced magnetocrystalline anisotropy in an ultra-dense array of air-exposed crystalline cobalt nanowires

Cite as: Appl. Phys. Lett. **109**, 202406 (2016); <https://doi.org/10.1063/1.4967982>

Submitted: 24 June 2016 . Accepted: 05 November 2016 . Published Online: 18 November 2016

I. S. Camara , C. Achkar, N. Liakakos, A. Pierrot, V. Pierron-Bohnes, Y. Henry, K. Soulantica , M. Respaud, T. Blon, and M. Bailleul



View Online



Export Citation



CrossMark

ARTICLES YOU MAY BE INTERESTED IN

[Vector network analyzer measurement of the amplitude of an electrically excited surface acoustic wave and validation by X-ray diffraction](#)

Journal of Applied Physics **121**, 044503 (2017); <https://doi.org/10.1063/1.4974947>

[Magnetization reversal in ferromagnetic spirals via domain wall motion](#)

Applied Physics Letters **109**, 202405 (2016); <https://doi.org/10.1063/1.4968012>

[Voltage-impulse-induced dual-range nonvolatile magnetization modulation in metglas/PZT heterostructure](#)

Applied Physics Letters **109**, 202903 (2016); <https://doi.org/10.1063/1.4967980>



Measure Ready
M91 FastHall™ Controller

A revolutionary new instrument
for complete Hall analysis

 Lake Shore
CRYOTRONICS



Enhanced magnetocrystalline anisotropy in an ultra-dense array of air-exposed crystalline cobalt nanowires

I. S. Camara,^{1,a)} C. Achkar,² N. Liakakos,² A. Pierrot,² V. Pierron-Bohnes,¹ Y. Henry,¹ K. Soulantica,² M. Respaud,² T. Blon,² and M. Bailleul^{1,b)}

¹*Institut de Physique et Chimie des Matériaux de Strasbourg, UMR 7504 CNRS, Université de Strasbourg, 23 rue du Loess, BP 43, 67034 Strasbourg Cedex 2, France*

²*Université de Toulouse, INSA, UPS, LPCNO, CNRS-UMR 5215, 135 avenue de Rangueil, 31077 Toulouse, France*

(Received 24 June 2016; accepted 5 November 2016; published online 17 November 2016)

The magnetic anisotropy of an ultradense array of crystalline cobalt nanowires is investigated by means of broadband ferromagnetic resonance and magnetic torque measurements. The array is grown epitaxially in solution on a Pt(111) film and consists of single crystalline metallic wires with a diameter of 6.2 nm and a center-to-center interwire distance of 9.6 nm. The shape anisotropy and the Co hexagonal compact structure with the *c*-axis along the wire axis combine with each other to impose a perpendicular magnetic anisotropy despite the high density of 8×10^{12} wires/in.². The intrinsic uniaxial magnetocrystalline anisotropy constants K_1 and K_2 are extracted from the ferromagnetic resonance and torque measurements using a mean field approach accounting for the interwire dipolar interactions. At room temperature, and despite air exposure, an unexpected increase of K_1 and K_2 of more than 40% with respect to the bulk is evidenced. *Published by AIP Publishing.*
[\[http://dx.doi.org/10.1063/1.4967982\]](http://dx.doi.org/10.1063/1.4967982)

Ferromagnetic nanowire (NW) arrays have been extensively studied due to their potential applications in microwave engineering¹ and magnetic recording.² In the latter field, conventional media are expected to reach their intrinsic limitations at around 1 Tbits/in.² due to superparamagnetic fluctuations.³ Intensive research is then carried out to design dense assemblies of nanomagnets, such as bit patterned media, where each bit consists of a single magnetic object of high magnetic anisotropy.⁴ In the field of microwave engineering, the ferrite materials used to fabricate non-reciprocal devices such as circulators also reach their limitations, mostly in terms of maximum frequency. From this point of view, self-biased assemblies of NWs constitute a promising alternative, with operating frequencies naturally in the range of several tens of GHz.¹ Arrays of NWs are traditionally prepared by electrodeposition in nanoporous templates,^{5,6} which results in polycrystalline objects arranged into assemblies of moderate densities, thus limiting their applicability. These nanomaterials often do not reach the strong anisotropy that could be expected when summing up the magnetocrystalline and shape anisotropies. The NWs investigated in this paper consist of a single-crystal cobalt. They are obtained by adapting the seed-mediated solution phase synthesis of nanocrystals⁷ to grow them epitaxially directly on crystalline thin films.⁸ On Pt(111), this method leads to the epitaxial growth of vertical wires with the *c*-axis of the hexagonal compact (*hcp*) structure parallel to the NW axis.⁹ The Co NWs spontaneously self-assemble into hexagonal arrays of 8×10^{12} NWs/in.² which, despite strong interwire dipolar interactions, exhibit a perpendicular magnetic anisotropy (i.e., with a magnetic easy axis parallel to the NWs) with a coercive field of 0.35 T at 300 K thanks to the combined effect of

uniaxial shape and magnetocrystalline anisotropies of the individual wires.⁹ The quantification of dipolar interactions in such dense assemblies is a complex problem which impedes the accurate determination of the fundamental figure of merit of individual nanowires, namely, their magnetocrystalline anisotropy (MCA). In this work, we present a comprehensive analysis of the magnetic anisotropy in our ultra-dense array of single-crystal Co NWs, with the use of broadband ferromagnetic resonance (FMR) and magnetic torque (MT) measurements. Experimental data are analysed by accounting precisely for interwire dipolar interactions using a mean field approach.

The array under study consists of metallic NWs of length $L = 1000 \pm 80$ nm and diameter $D = 6.2 \pm 0.8$ nm.⁸ Each NW is naturally covered with organic surfactants. Small angle neutron scattering measurements on air-exposed NWs yield a center-to-center interwire distance of $d = 9.6 \pm 0.5$ nm corresponding to a packing fraction $P = (\pi/2\sqrt{3}) \times (D/d)^2 = 0.38$.⁹ For the sample under study, a partial oxidation due to air exposure is revealed by the presence of a Co/CoO exchange bias field in the low temperature hysteresis loops (below 50 K) and by a 25% decrease of the room temperature saturation magnetic moment with respect to the value measured right after growth [see [supplementary material](#)]. Figure 1 shows the geometry of the FMR measurement performed at room temperature and in air, where the sample sits on top of a broadband channelized coplanar waveguide transducer with the magnetic layer facing it. A microwave vector network analyzer is used to feed the waveguide with microwaves and to measure its transmission coefficient S_{21} as a function of the microwave frequency $f = 1\text{--}50$ GHz and of the external magnetic field H_0 in the range of -2.7 to $+2.7$ T. This is converted into a dimensionless quantity $U = i \times \ln(S_{21}/S_{21}^{\text{ref}}) / \ln(S_{21}^{\text{ref}})$,¹⁰ which describes the magnetic response of the portion of waveguide covered with the

^{a)}Electronic mail: ibrahima.s.camara@gmail.com

^{b)}Electronic mail: matthieu.bailleul@ipcms.unistra.fr

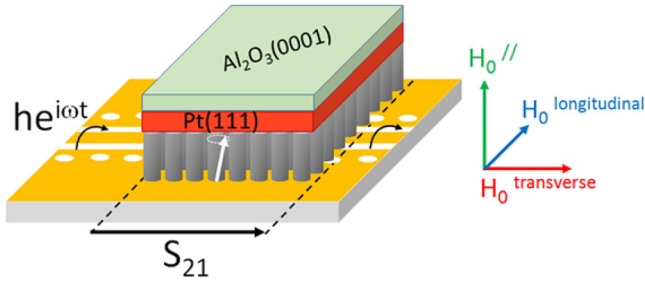


FIG. 1. Schematic of the channelized coplanar waveguide broadband FMR transducer with the Co nanowire array on top. The arrows on the right hand side indicate the three orientations of the static field H_0 investigated experimentally.

sample. Here S_{21}^{ref} is measured under a high magnetic field H_{ref} . As sketched in Fig. 1, the experiment is performed for three different directions of the applied field H_0 .

Figure 2(a) shows $\text{Im}(U)$, which is proportional to the microwave absorption of the sample, as a function of the frequency when the applied field is parallel to the NWs, i.e.,

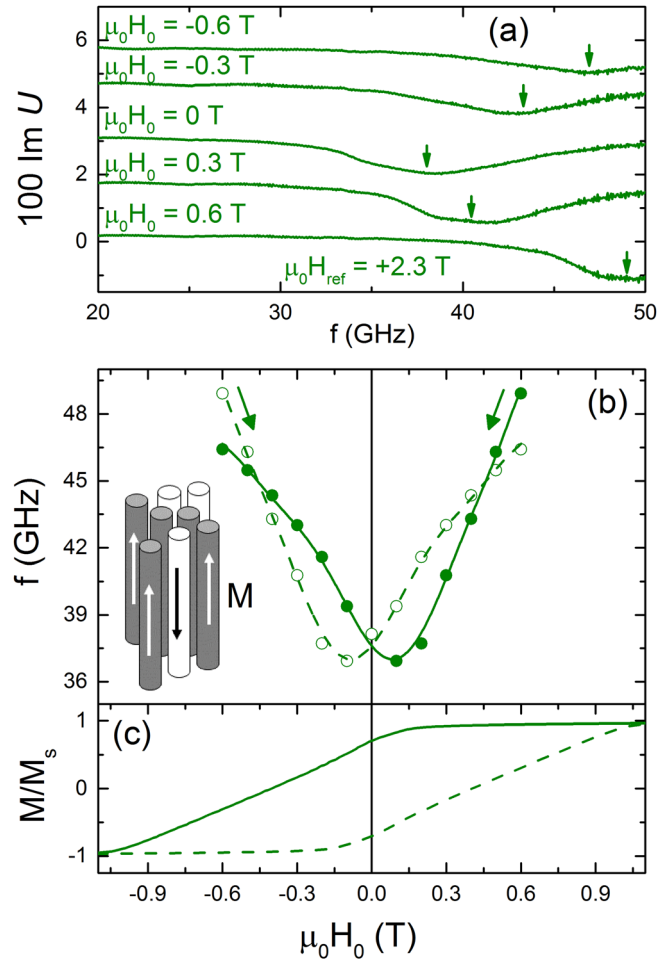


FIG. 2. (a) FMR spectra of the Co NW array at applied fields ranging from +0.6 to -0.6 T, oriented parallel to the NW axis, after application of a reference field $\mu_0 H_{\text{ref}} = +2.3$ T. (b) Experimental (circles) and calculated (lines) FMR frequency versus applied field. The full line and solid circles are for a field sweep from +2.3 to -2.3 T and describe the FMR frequency of NWs having their magnetization pointing upwards. The dashed line and open circles correspond to downward-magnetized NWs and a field sweep from -2.3 to 2.3 T. (c) Major hysteresis loop measured for an applied field H_0 parallel to the NW axis.

parallel to the magnetic easy axis. After application of $\mu_0 H_{\text{ref}} = +2.3$ T, the field is decreased to +0.6 T and then down to -0.6 T in 0.1 T steps. An intense and broad peak appears above 30 GHz in each spectrum, which we attribute to the microwave power absorbed by the Co NWs at the FMR frequency. The very large line-width of the peaks (about 5 GHz) is attributed to an inhomogeneous broadening arising from the inhomogeneity of the array [misalignment of some nanowires⁸ and/or dispersion of the local effective fields]. The solid circles in Figure 2(b) show the variation of the resonance frequency as a function of the applied field H_0 , as deduced from a Lorentzian fit of the spectra. Two regimes can be distinguished. Starting at large positive field, the frequency first decreases linearly with decreasing field. Then it reaches a minimum at about 0.1 T and starts to increase as the field is decreased further toward negative values. This can be explained considering the magnetization curve shown in Fig. 2(c): above 0.2 T, the sample is fully saturated along the applied field and the resonance frequency follows the Kittel formula $f = (\gamma\mu_0/2\pi) \times (H_0 + H_{K,\text{tot}})$, where μ_0 is the permeability of free space, γ is the gyromagnetic ratio, and $H_{K,\text{tot}}$ is the total magnetic anisotropy field acting on each NW in the saturated state. This effective field has contributions from the MCA field and from the intrawire and interwire dipolar fields. Below 0.1 T, the sample is no more saturated and $H_{K,\text{tot}}$ is no more constant, as the interwire dipolar field then varies with the applied field. In order to perform a more quantitative analysis of $f(H_0)$, we adapt the approach of Carignan *et al.*¹¹ to include MCA in it. We assume that the system is composed of two populations of NWs having their magnetization pointing upwards and downwards, respectively. For long NWs ($L \gg d, D$), the dipolar interactions between NWs can be described in a mean-field approximation.^{11,12} Solving the coupled Landau-Lifshitz-Gilbert (LLG) equations for the two populations leads to the following resonance conditions:

$$f_{\pm} = \pm \frac{\mu_0 \gamma H_0}{2\pi} + \frac{1}{2} \frac{\mu_0 \gamma M_s}{2\pi} \left\{ \left[1 - P + \left(\frac{\Delta n P}{2} \right)^2 + 4 \frac{H_{K1}^2}{M_s^2} + 4 \frac{H_{K1}}{M_s} \left(1 - \frac{P}{2} \right) \right]^{1/2} \mp \frac{5}{2} \Delta n P \right\}, \quad (1)$$

where + and - correspond to NWs magnetized upwards and downwards, respectively, and $\Delta n = n_+ - n_- = M/M_s$ is given by the hysteresis curve shown in Fig. 2(c). Here $H_{K1} = 2K_1/\mu_0 M_s$, where K_1 is the first order uniaxial MCA constant, and P is the array packing fraction. One retrieves easily the expression $H_{K,\text{tot}} = H_{K1} + M_s(1 - 3P)/2$ at saturation, i.e., for $\Delta n = \pm 1$. The measured FMR frequencies can be fitted to Eq. (1) with the following set of parameters: $\gamma/2\pi = 30$ GHz/T, $\mu_0 M_s = 1.8$ T, $P = 0.38$ and $K_1 = (7.4 \pm 0.1) \times 10^5$ J/m³ [see Fig. 2(b)], where the solid line (resp. dashed line) is obtained using the expression of f_+ (resp. f_-) [see [supplementary material](#) for a plot on a broader field and frequency range]. Note that this value of K_1 is 40% higher than the bulk value of hcp cobalt.^{13,14}

Let us now discuss the FMR spectra measured with the external field \mathbf{H}_0 applied perpendicularly to the nanowires. Two configurations are considered, which differ in the orientation of \mathbf{H}_0 with respect to that of the microwave field \mathbf{h} [Fig. 1]: the longitudinal configuration, where $\mathbf{H}_0 \parallel \mathbf{h}$, and the transverse one, where $\mathbf{H}_0 \perp \mathbf{h}$. In the two situations, the FMR spectra are recorded by sweeping the applied field for several fixed frequencies [see Figs. 3(a) and 3(b)]. Fig. 3(c) shows a plot of the peak frequency as a function of the resonance fields (as extracted from Lorentzian fits) for the two configurations. Starting at $\mu_0 H_0 = +2.7$ T, in the transverse configuration, the frequency first decreases with decreasing field, then it reaches a minimum at about 2.2 T and starts to increase as the field is decreased further (note that the weak features below 1.7 T are not attributed to the Co NWs themselves, see [supplementary material](#)). For the longitudinal configuration, there is no resonance visible at high field. The FMR peak appears first when the field is decreased to about 2 T, and its amplitude and frequency increase as the field is decreased further. The change of amplitude is attributed to the fact that the coupling between the magnetization and the microwave field vanishes when they are parallel to each other, which is expected to happen for a strong enough field in the longitudinal configuration. In order to obtain the theoretical frequency-field relations, we adapt the approach of Boucher *et al.*¹⁵ to include MCA. Because of the mirror symmetry of the system with respect to its median horizontal plane, we assume that, below saturation, the NWs split into two populations of equal fraction $n_1 = n_2 = 1/2$ with their equilibrium magnetization lying at the same angle θ with respect to the upward and downward NW axis, respectively [see the inset in Fig. 3(c)]. Solving the two coupled LLG equations, we find the following resonance conditions:

$$f_{\perp}^{\parallel} = \frac{\mu_0 \gamma}{2\pi} \left\{ \left[H_0 \sin \theta + H_{k1} \cos^2 \theta + H_{k2} \sin^2 \theta \cos^2 \theta + \frac{1-P}{2} M_s \cos^2 \theta + \frac{1 \pm 1}{4} P M_s \right] \times \left[H_0 \sin \theta + H_{k1} \cos 2\theta + H_{k2} \sin^2 \theta (1 + 2 \cos 2\theta) + \frac{4 - (7 \pm 1)P}{8} M_s \cos 2\theta + \frac{5 \mp 1}{8} P M_s \right] \right\}^{1/2}, \quad (2)$$

where the subscript \parallel (resp. \perp) refers to the acoustic (resp. optic) precession mode expected to be visible in the longitudinal (resp. transverse) configuration. Here $H_{k2} = 4K_2/\mu_0 M_s$, where K_2 is the second order uniaxial MCA constant,¹⁶ and θ is the equilibrium angle given by $H_0 - [H_{k1} + M_s(1-P)/2] \sin \theta - H_{k2} \sin^3 \theta = 0$. The data points in Fig. 3(c) can be fitted correctly to Eq. (2) using $K_2 = (1.8 \pm 0.2) \times 10^5$ J/m³ and the value of K_1 derived in the $\mathbf{H}_0 \parallel$ NW configuration. With these values, the magnetization curve deduced from the equilibrium condition given above is also in correct agreement with the measured one [Fig. 3(d)], and the saturation field $H_{\text{sat}} = H_{K1} + H_{K2} + M_s(1-P)/2$ amounts to 2.2 T.

The values of K_1 and K_2 have also been derived from magnetic torque (MT) measurements¹⁷ carried out with external magnetic fields large enough to ensure that the nanowire assembly is magnetized to saturation. The experiments consist in recording the variation of the magnetic anisotropy torque $\Gamma_a = -\partial E_a / \partial \theta$, deriving from the anisotropy energy E_a , while the applied field is rotated in a plane parallel to the NW axis. In such an experimental geometry, the relevant anisotropy energy writes $E_a/V = K_1^{\text{tot}} \sin^2 \theta + K_2 \sin^4 \theta$, where V is the total magnetic volume, $K_1^{\text{tot}} = K_1 + \mu_0 M_s^2(1-3P)/4$ is an effective first order uniaxial anisotropy constant containing crystal and dipolar contributions, and θ is the angle of the

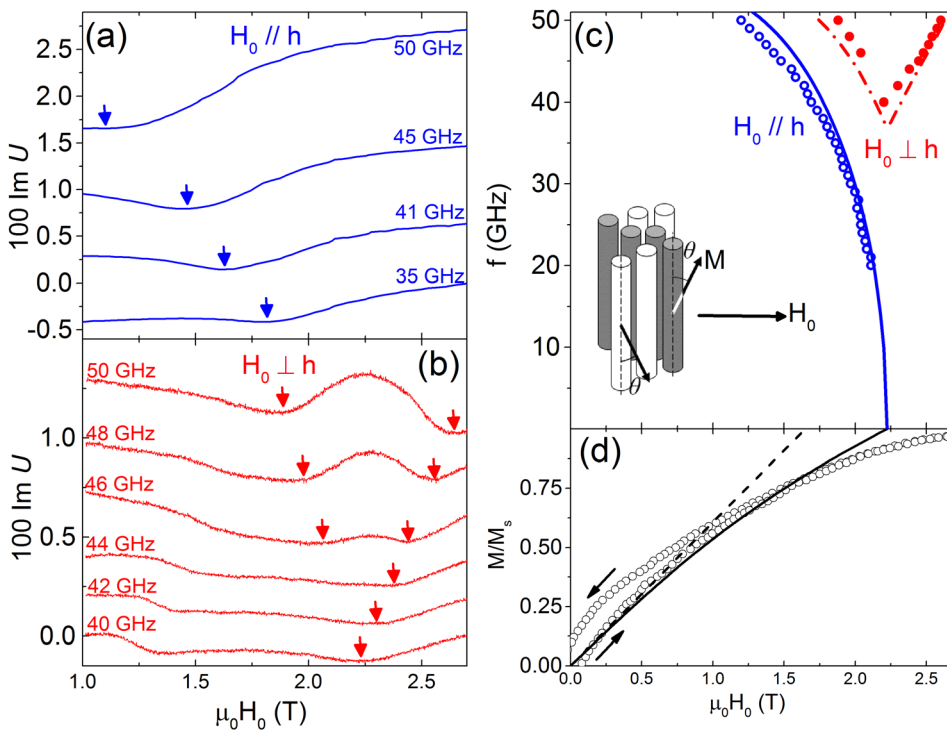


FIG. 3. FMR spectra of the Co NW array for an applied field \mathbf{H}_0 perpendicular to the NW axis, in (a) the longitudinal configuration, $\mathbf{H}_0 \parallel \mathbf{h}$, and in (b) the transverse configuration, $\mathbf{H}_0 \perp \mathbf{h}$. (c) Experimental (circles) and calculated (lines) FMR frequency versus field. The solid line and open circles are for the longitudinal configuration and the dot-dashed line and solid symbols are for the transverse one. (d) Measured (circles) and calculated (lines) magnetization loops for an external applied field \mathbf{H}_0 perpendicular to the NWs. The solid and dashed lines are calculated for $K_2 = 1.8 \times 10^5$ J/m³ and $K_1 = 0$, respectively.

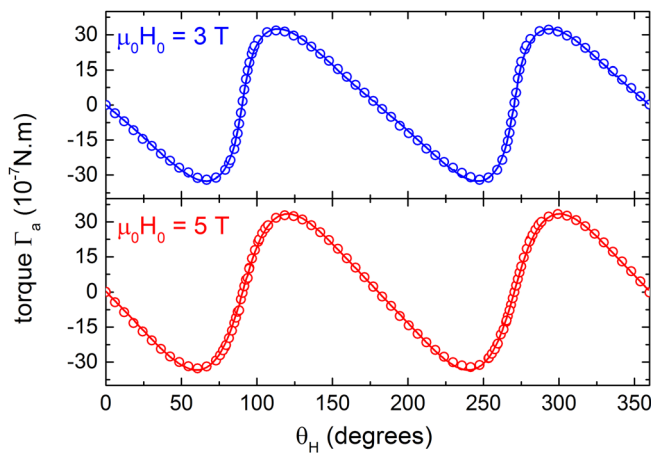


FIG. 4. Magnetic anisotropy torque measured at 3 T and 5 T (circles) and fits to Eq. (3) (lines). θ_H is the angle of the applied field with respect to the NW axis.

magnetic moment of the NW assembly, \mathbf{m} , as measured from the NW axis. The torque thus obeys

$$\frac{\Gamma_a(\theta)}{V} = -(K_1^{\text{eff}} + K_2)\sin 2\theta + \frac{K_2}{2}\sin 4\theta. \quad (3)$$

Correcting the measured torque curves $\Gamma_a(\theta_H)$ for the shear-distortion $\theta - \theta_H = \arcsin[\Gamma_a/(\mu_0 m H_0)]$ caused by the misalignment of the sample magnetic moment with respect to the applied field \mathbf{H}_0 (Ref. 18) and fitting the corrected data to Eq. (3), consistent values of $K_1 = (7.4 \pm 0.2) \times 10^5 \text{ J/m}^3$ and $K_2 = (2.9 \pm 0.2) \times 10^5 \text{ J/m}^3$ could be extracted from measurements at different values of the rotating field (Fig. 4).

Thus, MT and FMR measurements consistently confirm the high intrinsic anisotropy of the NWs despite their partial oxidation. This is attributed to the high crystalline order of the metallic part of the NWs. Unexpected high values of the first and second order MCA constants compared to those of bulk cobalt^{13,14} ($K_1 = 5.2 \times 10^5 \text{ J/m}^3$, $K_2 = 1.0 \times 10^5 \text{ J/m}^3$) are extracted. One possible origin for the enhancement of the MCA with respect to the bulk is the magneto-elastic interaction.¹⁹ Using bulk Co values of the magneto-elastic coupling coefficients,¹⁹ an in-plane tensile strain $\varepsilon = +0.33\%$ would indeed explain an increase of K_1 of $2.2 \times 10^5 \text{ J/m}^3$. For epitaxial layers of *hcp* Co, increased MCAs have been observed and attributed to such tensile stress.^{20,21} The X-ray diffraction peaks measured on the present sample are however too broad to quantify such a small strain. The enhancement of the MCA can also be due to a surface anisotropy K_S on the sides of the nanowires, i.e., at Co/organic ligands (or possibly Co/CoO) interfaces. Based on a simple geometric consideration, assuming that the NWs are hexagonal with six facets of surface S , one gets a total surface anisotropy energy $E_S^{\text{tot}} = -3K_S S \sin^2 \theta$, which corresponds to a contribution per unit of volume $E_S^{\text{tot}}/V = -2/(\sqrt{3}a)K_S \sin^2 \theta$, where a is the width of a facet. For $a = D/2 = 3.1 \text{ nm}$, the observed increase of $2.2 \times 10^5 \text{ J/m}^3$ in K_1 leads to $K_S = -0.6 \text{ mJ/m}^2$, which is of the right order of magnitude for a 3d ferromagnetic surface.²²

In summary, we have shown that the broad band ferromagnetic resonance and magnetic torque are efficient tools to measure the intrinsic figure of merit of Co nanowires, even when packed in dense assemblies. At room temperature, the

first and second order MCA constants exceed those of bulk cobalt by more than 40%. This spectacular enhancement opens many questions concerning the temperature dependence of MCA in NWs, the role of core and surface magnetism, the influence of magneto-elastic effects and surface chemistry (oxidation rate). These results confirm the interest for the growth of single crystalline Co nanorods and nanowires, and for their integration in rare-earth-free magnets, magnetic memories, sensors, and microwave devices.

See [supplementary material](#) for additional information on the oxidation of the Co NWs and on the frequency-field FMR curves.

The authors would like to thank A. Boulard, B. Leconte, D. Spor (IPCMS) and O. Tantot (XLIM) for their assistance in building the FMR setup and C. Mény (IPCMS) for useful discussions. This work was supported by the Agence Nationale de la Recherche (France) under Contract Nos. ANR-11-BS10-003 (NanoSWITI) and ANR-14-CE07-0025-01 (DENSAR).

¹M. Darques, J. De la Torre Medina, L. Piraux, L. Cagnon, and I. Huynen, *Nanotechnology* **21**, 145208 (2010).

²L. Sun, Y. Hao, C.-L. Chien, and P. C. Searson, *IBM J. Res. Dev.* **49**, 79 (2005).

³H. Richter, A. Dobin, O. Heinonen, K. Gao, R. V. D. Veerdonk, R. Lynch, J. Xue, D. Weller, P. Asselin, M. Erden, and R. Brockie, *IEEE Trans. Magn.* **42**, 2255 (2006).

⁴Y. Shiroishi, K. Fukuda, I. Tagawa, H. Iwasaki, S. Takenoiri, H. Tanaka, H. Mutoh, and N. Yoshikawa, *IEEE Trans. Magn.* **45**, 3816 (2009).

⁵A. Huczko, *Appl. Phys. A* **70**, 365 (2000).

⁶M. Darques, A. Encinas, L. Vila, and L. Piraux, *J. Phys. D* **37**, 1411 (2004).

⁷K. Soulantica, F. Wetz, J. Maynadié, A. Falqui, R. P. Tan, T. Blon, B. Chaudret, and M. Respaud, *Appl. Phys. Lett.* **95**, 152504 (2009).

⁸N. Liakakos, C. Achkar, B. Cormary, J. Harmel, B. Warot-Fonrose, E. Snoeck, B. Chaudret, M. Respaud, K. Soulantica, and T. Blon, *ACS Nano* **9**, 9665 (2015).

⁹N. Liakakos, T. Blon, C. Achkar, V. Vilar, B. Cormary, R. P. Tan, O. Benamara, G. Chaboussant, F. Ott, B. Warot-Fonrose, E. Snoeck, B. Chaudret, K. Soulantica, and M. Respaud, *Nano Lett.* **14**, 3481 (2014).

¹⁰S. S. Kalarickal, P. Krivosik, M. Wu, C. E. Patton, M. L. Schneider, P. Kabos, T. J. Silva, and J. P. Nibarger, *J. Appl. Phys.* **99**, 093909 (2006).

¹¹L.-P. Carignan, C. Lacroix, A. Ouimet, M. Ciureanu, A. Yelon, and D. Ménard, *J. Appl. Phys.* **102**, 023905 (2007).

¹²V. Boucher, L.-P. Carignan, T. Kodera, C. Caloz, A. Yelon, and D. Ménard, *Phys. Rev. B* **80**, 224402 (2009).

¹³Z. Frait, *Br. J. Appl. Phys.* **15**, 993 (1964).

¹⁴D. Paige, B. Szpunar, and B. Tanner, *J. Magn. Magn. Mater.* **44**, 239 (1984).

¹⁵V. Boucher, C. Lacroix, L.-P. Carignan, A. Yelon, and D. Ménard, *Appl. Phys. Lett.* **98**, 112502 (2011).

¹⁶The FMR frequencies are found to depend on K_2 for the $H_0 \perp$ NW configuration but not for the $H_0 \parallel$ NW one. Indeed, for a MCA energy density $E_a = K_1 \sin^2 \theta + K_2 \sin^4 \theta$, the second order derivative of the second term is zero for $\theta = 0$.

¹⁷Y. Henry, K. Ounadjela, L. Piraux, S. Dubois, J.-M. George, and J.-L. Duvail, *Eur. Phys. J. B* **20**, 35 (2001).

¹⁸R. F. Pearson, "Magnetic anisotropy," *Experimental Magnetism*, edited by G. M. Kalvius and R. S. Tebble (John Wiley & Sons, 1979), Vol. 1, pp. 137–224.

¹⁹D. Sander, *J. Phys.: Condens. Matter* **16**, R603 (2004).

²⁰J. Prokop, D. A. Valdaitsev, A. Kukunin, M. Pratzner, G. Schönhense, and H. J. Elmers, *Phys. Rev. B* **70**, 184423 (2004).

²¹S. Boukari, E. Beaupaire, H. Bulou, B. Carrière, J. Deville, F. Scheurer, M. De Santis, and R. Baudouin-Savois, *Phys. Rev. B* **64**, 144431 (2001).

²²M. T. Johnson, P. J. H. Bloemen, F. J. A. D. Broeder, and J. J. D. Vries, *Rep. Prog. Phys.* **59**, 1409 (1996).